ADVANCED OPTICAL MATERIALS
www.advopticalmat.de

Efficient Sky-Blue Organic Light-Emitting Diodes Using a Highly Horizontally Oriented Thermally Activated Delayed Fluorescence Emitter

Zhen Zhang, Ettore Crovini, Paloma L. dos Santos, Bilal A. Naqvi, David B. Cordes, Alexandra M. Z. Slawin, Prakhar Sahay, Wolfgang Brütting, Ifor D. W. Samuel,* Stefan Bräse,* and Eli Zysman-Colman**

Organic thermally activated delayed fluorescent (TADF) materials can harvest 100% of the electrically generated excitons as a result of their small singlet–triplet energy difference. However, maximizing the external quantum efficiency (EQE) of a device also requires enhancing the light out-coupling efficiency. This work presents a new acceptor–donor–acceptor (ADA) emitter employing an indolocarbazole donor and diphenyltriazine acceptors that show nearly-completely horizontal orientation regardless of the host matrix, leading to a sky-blue organic light-emitting diode (λ_{EL} = 483 nm, CIE coordinates of 0.17, 0.32) with EQE_{MAX} of 22.1%, a maximum luminance of 7800 cd m^{-2}, and blue emission.

1. Introduction

Organic thermally activated delayed fluorescent (TADF) materials have become a competitive class of emitters capable of harvesting both singlet and triplet excitons to thus achieve up to 100% internal quantum efficiency (IQE) in organic light-emitting diodes (OLEDs).[1,2] In 2012, Adachi reported the first example of a highly efficient TADF OLED, with an IQE of 93% and a maximum external quantum efficiency, EQE_{max}, of 19.3%, employing a purely organic TADF emitter, 4CzIPN.[3] TADF molecules have an energy gap between the S_1 and T_1 states, ΔE_{ST}, sufficiently small to allow the triplet excitons to convert into singlet excitons through reverse intersystem crossing (RISC), making possible their radiative decay from the singlet excited state, evidenced by a delayed fluorescence. To minimize ΔE_{ST} and enhance k_{RISC}, the overlap between the highest occupied molecular orbital (HOMO) and lowest unoccupied molecular orbital (LUMO) of the molecule must likewise be small, which is achievable in compounds containing electron-donating and electron-accepting moieties that are poorly electronically coupled giving the excited state an intra-molecular charge-transfer (CT) character.[4] The most common emitter designs rely on a large twist angle between the donor and acceptor coupled with the incorporation of aromatic spacer bridging moieties.[5]

The external quantum efficiency (EQE) of the OLED is a function not only of the IQE but also of the light out-coupling efficiency. As the stack of an OLED device is composed of several different layers of materials included between two electrodes, total internal reflection at the interface between two media, and coupling to surface plasmon polaritons (SPP) at the interface with

Dr. Z. Zhang, Prof. S. Bräse
Institute of Organic Chemistry
Karlsruhe Institute of Technology (KIT)
Fritz-Haber-Weg 6, Karlsruhe 76131, Germany
E-mail: braese@kit.edu

E. Crovini, Dr. D. B. Cordes, Prof. A. M. Z. Slawin, Prof. E. Zysman-Colman
Organic Semiconductor Centre, EaStCHEM School of Chemistry
University of St Andrews
Fife, St Andrews KY16 9ST, UK
E-mail: eli.zysman-colman@st-andrews.ac.uk

The ORCID identification number(s) for the author(s) of this article can be found under https://doi.org/10.1002/adom.202001354.

DOI: 10.1002/adom.202001354

Dr. P. L. dos Santos, Prof. I. D. W. Samuel
Organic Semiconductor Centre, SUPA, School of Physics and Astronomy
University of St Andrews
North Haugh, St Andrews KY16 9SS, UK
E-mail: idws@st-andrews.ac.uk

B. A. Naqvi, P. Sahay, Prof. W. Brütting
Experimental Physics IV, Institute of Physics
University of Augsburg
Universitätsstr. 1, Augsburg 86159, Germany
E-mail: bruetting@physik.uni-augsburg.de

Prof. S. Bräse
Institute of Biological and Chemical Systems – Functional Molecular Systems (IBCS-FMS)
Karlsruhe Institute of Technology (KIT)
Hermann-von-Helmholtz-Platz 1, Eggenstein-Leopoldshafen
D-76344, Germany

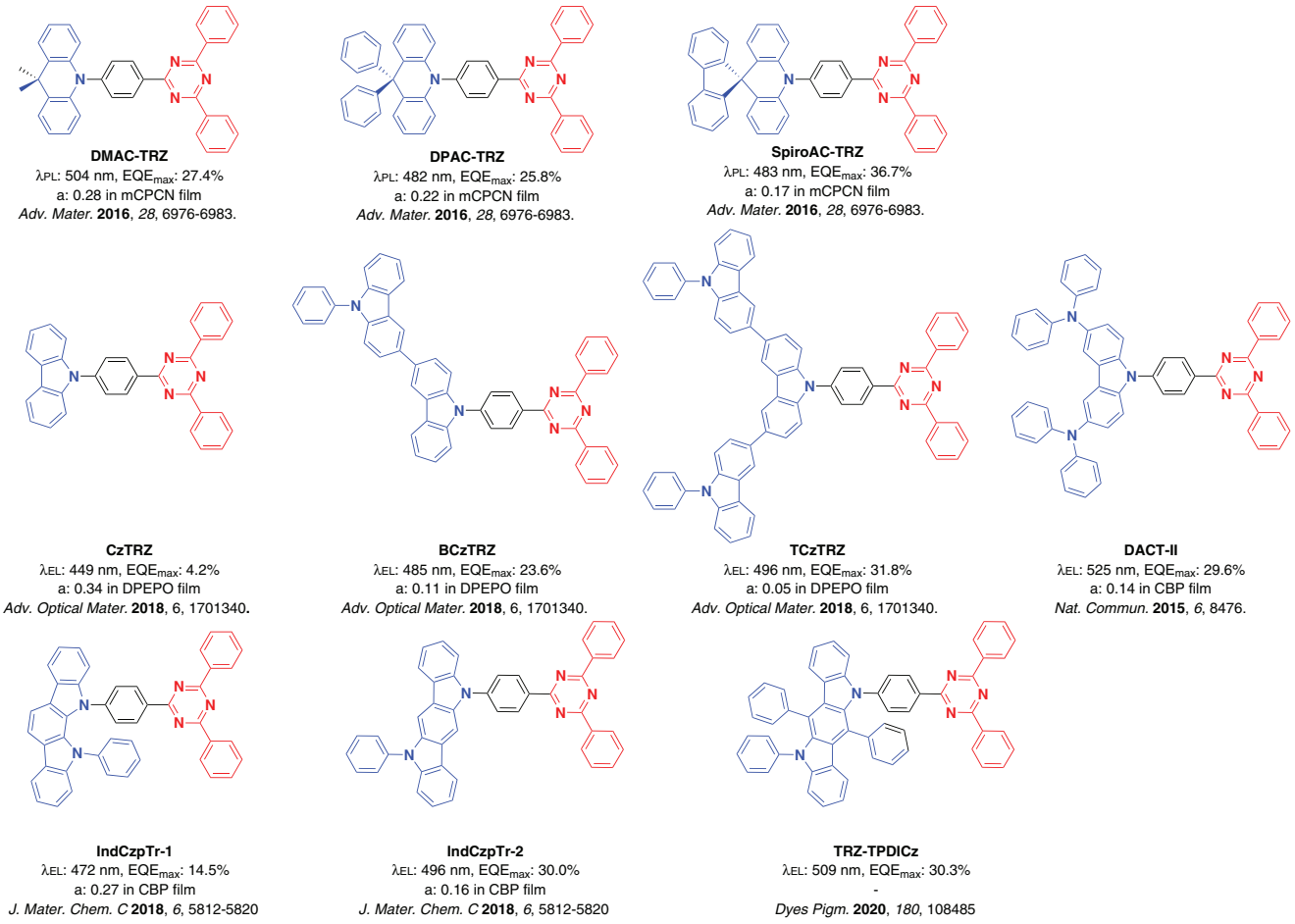

Figure 1. Chemical structures and performance of known triazine-based TADF emitters.

the cathode, can reduce the amount of generated light exiting the device to only about 25% of the light generated by the emitters. Since molecules emit most of the light in a perpendicular direction to their transition dipole moment (TDM), achieving horizontal orientation of the TDM of an emitter in a thin-film layer would maximize the amount of light exiting the device.

The design challenge now becomes a matter of trying to create an emitter that presents preferential horizontal orientation and good TADF properties in terms of a small singlet–triplet energy gap (ΔE_{ST}) and fast reverse intersystem crossing rates. Yokoyama et al. showed that longer molecules and the introduction of terminal bulky groups lead to a compound with a higher degree of horizontal orientation.[6] Diphenyltriazine has been employed as an acceptor group in many highly oriented TADF emitters (**Figure 1**). Lyn et al. studied the relationship between structure and the propensity for the emitter to be horizontally oriented in several acridine-triazine derivatives. Doped films of DMAC-TRZ, DPAC-TRZ, and SpiroAC-TRZ in mCPCN[7] matrices show orientations from isotropic to horizontal with anisotropy factor values (see below), *a*, of 0.28, 0.22, and 0.17, respectively, showing the positive effect that bulkier groups at the terminus of the molecule have on the orientation of the emitter. Herein, the anisotropy factor *a* is defined as the fraction of power emitted by vertical dipoles, with a value of 0.33 indicating isotropic dipole orientation and 0 denoting perfectly horizontal alignment.[8] Note that different conventions and terminology are used to quantify anisotropy of the TDM orientation in light-emitting devices. The parameter used here *a* (or synonymously $\Theta_v = \langle\cos^2\vartheta\rangle$) denotes the second moment of the TDM's angular distribution around the surface normal of the film, where ϑ is the angle between the molecule's TDM vector and the said direction.

This strategy was also employed by Beyon, Kaji, et al. where they reported four carbazole-based emitters CzTRZ, BCzTRZ, TCzTRZ,[9] and DACT-II.[10] Orientation becomes progressively more horizontal with increasing number of pendant carbazoles on the donor. CzTRZ (a = 0.34) is isotropically oriented while there is almost complete horizontal orientation in TCzTRZ (a = 0.05); DACT-II is preferentially horizontally aligned (a = 0.14), and the OLED employing this emitter reached an EQE_{max} of 29.6%. Xiang et al. and Maeng et al. incorporated the more planar and rigid ICz (indolocarbazole) donor in IndCzpTr1 and IndCzpTr2,[11] and TRZ-TPDICz,[12] respectively, achieving high EQE_{max} values of 14.5%, 30%, and 30.3%, respectively, due in part to the preferential horizontal orientation of these emitters. Indolocarbazole has been previously employed in TADF emitter design as the donor moiety in a small number of reports, although none of these cases showed a di-functionalized ICz unit.[13–16] Here, we report the first

example of a di-functionalized ICz-based A-D-A TADF emitter. The ICz donor was selected due to its planar and rigid structure, suitable electron-donating strength and the possibility to functionalize the two nitrogen atoms of the donor to obtain a longer and linear structure with the expectation to achieve a horizontal orientation.[6,17] By adding a second acceptor onto the ICz donor, this should lead to an increased HOMO-LUMO gap and a blue-shifted emission than the previously published mono-functionalized emitters employing the ICz moiety.[11,12,18] Indeed, ICzTRZ shows both very high photoluminescence quantum yield and strongly horizontally oriented transition dipole moments (TDMs) and demonstrates its potential in a highly efficient sky-blue OLED.

2. Results and Discussion

Building upon previously described TADF emitters possessing an ICz donor group, we designed ICzTRZ to include a central 5,11-dihydroindolo[3,2-b]carbazole, ICz, donor coupled to two 2,4-bis(4-*tert*-butylphenyl)-1,3,5-triazine, TRZ, acceptors. The *tert*-butyl groups were incorporated onto the acceptors to: 1) enhance solubility; 2) extend the effective length and bulkiness of the target emitter in order to reduce the propensity for aggregation-caused quenching; 3) enhance the likelihood that the emitter would be horizontally oriented; and 4) tune the electron-withdrawing strength of the TRZ group.[19,20] The indolocarbazole possesses an excellent charge-transporting ability and its greater conjugation leads to an enhanced donor strength when compared to the more commonly used carbazole. The latter is evidenced by DFT calculations run on CzPh-TRZ (also known as Cz-TRZ) and IndCzpTr-2,[11] where the HOMO energy level is higher for the ICz based molecule (−5.14 vs −5.64 eV for the Cz based one).

2.1. Synthesis

The target molecule, ICzTRZ (**Figure 2**a), was synthesized following a three-step procedure (**Scheme 1**). First, the triazine acceptor **1** was obtained through the Grignard reaction of two equivalents of *tert*-butylphenyl magnesium bromide with 2,4,6-trichloro-1,3,5-triazine. Next, a 4-fluorophenyl group was added to **1** using Suzuki-Miyaura cross-coupling to afford **2**. The indolocarbazole donor, ICz, was obtained via an acid-promoted cyclization of 3,3-diindolylmethane on a multigram scale. Nucleophilic aromatic substitution, using tripotassium phosphate as the base, of **2** with ICz afforded ICzTRZ in good yield. The emitter was fully characterized by ^{1}H NMR, ^{13}C NMR, HRMS, IR, Mp, and EA. The structure of ICzTRZ was determined by single crystal X-ray diffraction (Figure 2b). The molecule shows a 46.5° dihedral angle between the ICz and the adjacent phenyl ring of the TRZ acceptor, similar to conformation found in CzPhTRZ,[21] which has a dihedral angle of 45.1°. There are two independent molecules in the asymmetric unit and these show π–π stacking between the central benzene ring of the ICz donors and the triazine ring of the acceptors of each of the two independent molecules, at centroid···centroid distances of 3.70 and 3.76 Å.

2.2. Theoretical Calculations

Density functional theory (DFT) and time-dependent DFT (TD-DFT) calculations at the PBE0/6-031G(d,p) level revealed the promise of ICzTRZ as a TADF emitter (**Figure 3**). The ground-state geometry optimization was carried out in the gas phase. The nature of the S_1 and T_1 states and their corresponding energies were then obtained using the Tamm-Dancoff approximation (TDA)[22] to TD-DFT. ICzTRZ possesses a ΔE_{ST} of 0.22 eV and an S_1 energy of 2.92 eV. The high oscillator strength (*f*) of 0.72 is helpful for favoring radiative decay. There are additionally two intermediate triplet excited states residing between S_1 and T_1, which is beneficial as it has previously been shown that a density of triplet states can mediate a vibrationally assisted reverse internal conversion that leads to an enhanced efficiency RISC process.[23–27] The T_3 state is locally excited in nature (see Table S1, Supporting Information) and thus RISC from T_3 to S_1 will be facile according to El-Sayed's rule.[28] The HOMO and LUMO of the molecule are mainly localized, respectively, on the donor and the acceptor moieties. ICzTRZ presents a small permanent dipole moment (PDM) of 0.3 Debye, but a much larger transition dipole moment (TDM) of 7.9 Debye.

2.3. Optoelectronic Properties

We first studied the electrochemical properties of ICzTRZ in degassed DCM with tetra-*n*-butylammonium hexafluorophosphate as the electrolyte and Fc/Fc^{+} as the internal reference

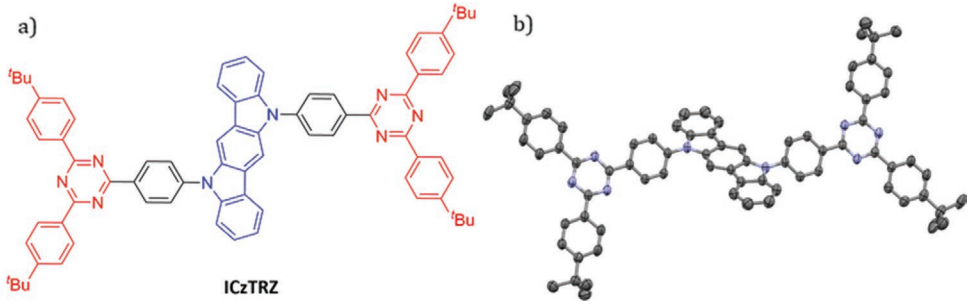

Figure 2. a) Chemical structure of ICzTRZ. b) View of the crystal structure of one independent molecule of ICzTRZ, ellipsoids drawn at the 50% probability level, hydrogen atoms and solvent omitted for clarity.

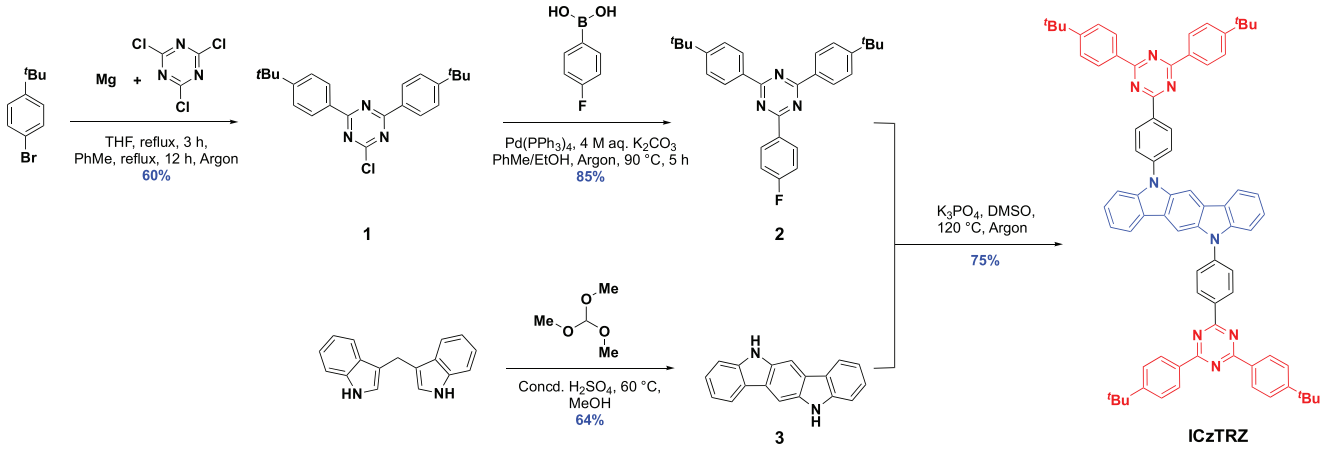

Scheme 1. Synthetic route to ICzTRZ.

(**Figure 4**a). Unlike what is typically observed for carbazole-based oxidations, which are known to be irreversible,[21,29–32] we observed a reversible oxidation wave with E_{ox} at 0.96 V measured from the DPV. By contrast, the reduction wave at −1.83 V is irreversible. The corresponding HOMO and LUMO levels inferred from the DPV are −5.66 eV and −3.17 eV, respectively.

The UV–vis absorption spectrum in toluene coincides broadly with the absorption spectra of other indolocarbazole-based compounds (Figure 4b).[11] There are a number of high-intensity absorption bands from 280 to 350 nm that are assigned both to charge-transfer (CT) transitions (for the bands at 321 nm and 331 nm) and locally excited (LE) transitions on the indolocarbazole (for the band at 340 nm) (confirmed by DFT calculations, see Table S3, Supporting Information). There are low intensity bands around 400 nm that are assigned to a charge-transfer (CT) transition between the ICz and the TRZ acceptor moieties. In the ground state, there is a small dipole, supported by DFT calculations (see Figure 3), reflective of the lack of solvatochromism present in the absorption spectra (Figure 4d). This can be understood by the cancellation of the large CT dipoles that originate from the transitions from the ICz to the TRZ. The photoluminescence (PL) spectrum in toluene is broad and unstructured, indicating an emission from a CT state, which was expected from the large TDM calculated from TDA-DFT (see Figure 3). The emission maximum, λ_{PL}, is centered at 462 nm in toluene. The PL spectra are sensitive to solvent polarity. With increasing solvent polarity from toluene to DCM, there is a characteristic red-shifting of the emission coupled with a broadening of the spectrum. However, in methylcyclohexane (least polar solvent), the emission is structured, reflecting a radiative decay from a LE state on the ICz moiety, also predicted from DFT calculations (see Figure S10, Supporting Information).

Transient PL measurements in degassed toluene showed monoexponential decay kinetics with τ_p of 9.0 ns for the prompt fluorescence and τ_d of 229.2 µs for the delayed fluorescence. Upon exposure to oxygen, the delayed emission could no longer be detected. The Φ_{PL} in degassed toluene was high at 72%, which decreased to 56% after the solution was exposed to air (**Table 1**).

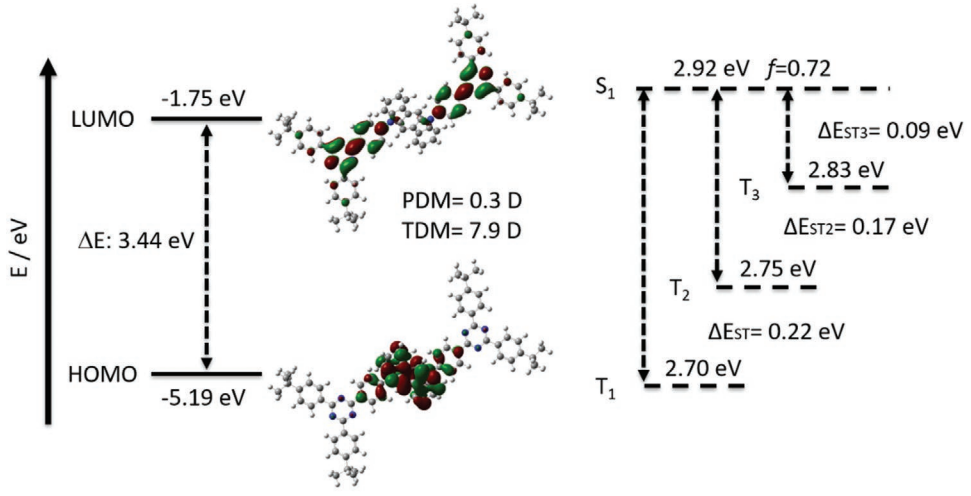

Figure 3. HOMO and LUMO electron density distributions and energy levels (in eV), excited state energy levels (in eV), and calculated permanent (PDM) and transition dipole moments (TDM) of ICzTRZ.

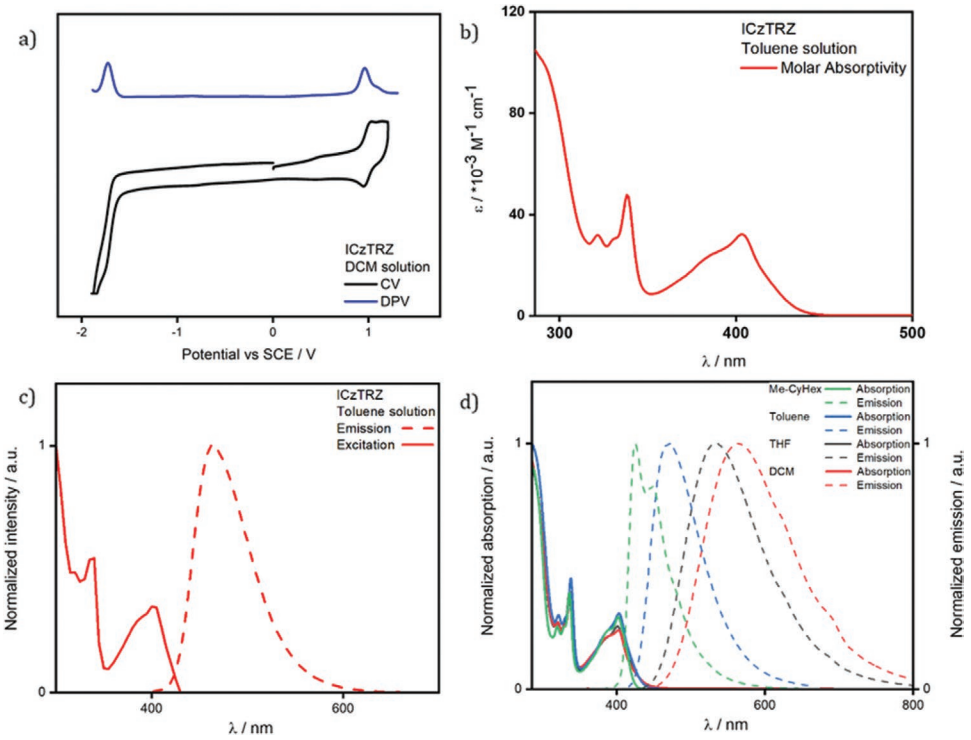

Figure 4. a) Cyclic voltammetry (CV) and differential pulse voltammetry (DPV) of ICzTRZ in DCM (scan rate = 100 mV s^{-1}). b) UV–vis absorption spectrum of ICzTRZ in toluene. c) Emission and excitation spectra of ICzTRZ (10^{-5} M toluene solution, λ_{exc} = 360nm). d) Ground and excited state solvatochromism study of ICzTRZ (λ_{exc} = 340 nm).

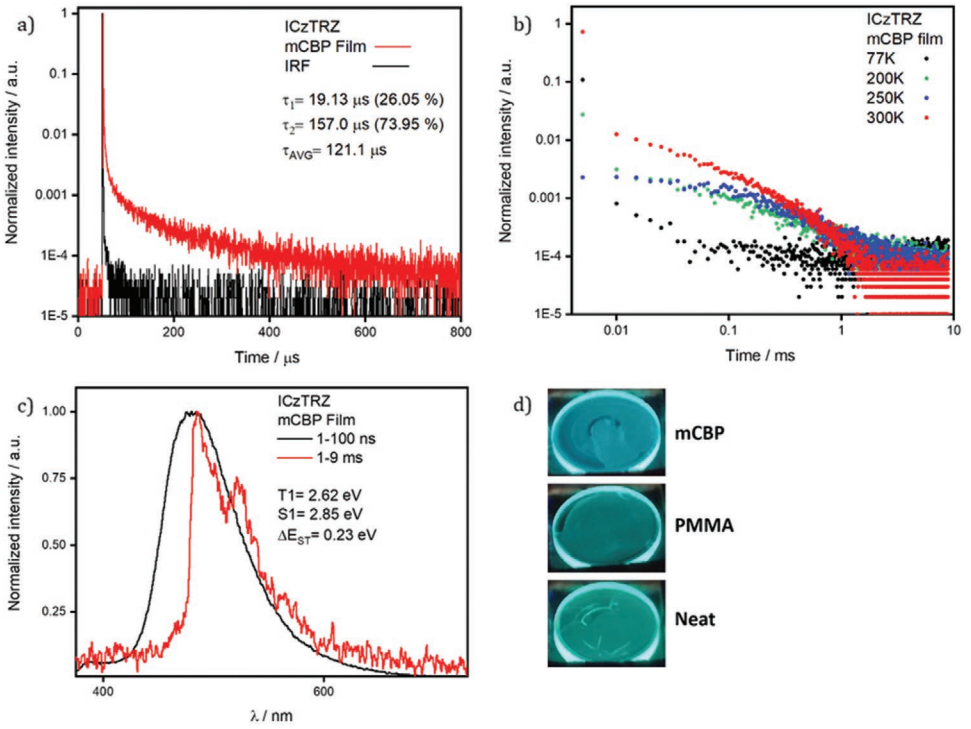

Figure 5. a) Delayed fluorescence decay of a spin-coated film of 5 wt% of ICzTRZ in mCBP (λ_{exc} = 340 nm). b) Temperature dependence of the delayed component (λ_{exc} = 340 nm). c) Prompt fluorescence spectra (77 K) and phosphorescence spectra (77 K) measured with an iCCD camera used to determine the S_1 and T_1 energy levels (λ_{exc} = 343 nm, prompt and delayed fluorescence spectra were obtained in the 1–100 ns and 1–9 ms time range, respectively). d) Pictures of spin-coated films in different host materials under UV excitation.

Table 1. Photophysical properties of ICzTRZ in degassed toluene solution (10^{-5} M), 5 wt% doped mCBP film, and 10 wt% doped PMMA film.

Environment	λ_{PL} [nm][a,b]	Φ_{PL} air; N_2[b,c] [%]	τ_p; τ_d[d] [ns; µs]	S_1[e] [eV]	T_1[f] [eV]	ΔE_{ST}[g] [eV]
Toluene (10^{-5} M)	462	56; 72[c]	9.0; 229.2	2.94	2.62	0.32
mCBP 5 [wt%]	479	59; 70	8.7; 121.1	2.85	2.62	0.23
PMMA 10 [wt%]	470	28; 31	11.5; 252.8	2.75	2.64	0.11

[a]Measured at room temperature; [b]λ_{exc} = 340 nm; [c]Obtained via the optically dilute method (see Supporting Information), λ_{exc} = 360 nm; [d]τ_p (prompt lifetime) and τ_d (delayed lifetime) were obtained from the transient PL decay of degassed solution/doped film, λ_{exc} = 378 nm; [e]S_1 was obtained from the onset of the prompt emission measured at room temperature; [f]T_1 was obtained from the onset of the phosphorescence spectrum measured at 77 K; [g]$\Delta E_{ST} = S_1 - T_1$.

We next investigated the solid-state photophysical behavior in a number of different host matrices (Table 1). We started by spin-coating 10 wt% doped film in PMMA to study ICzTRZ in a non-polar matrix. The film presented emission in the blue region at λ_{PL} of 470 nm and a Φ_{PL} of 31% under N_2. Transient PL measurements were then carried out (**Figure 5**). A prompt fluorescence (see Figure S13, Supporting Information) with a biexponential decay kinetics and an average τ_p of 11.5 ns [τ_1 = 7.6 ns (62%), τ_2 = 17.6 ns (38%)], and a delayed component with a biexponential decay with an average τ_d of 252.8 µs [τ_1 = 85.5 µs (51%), τ_2 = 427.3 µs (49%)] were observed. A study involving a range of hosts and concentrations then revealed that the Φ_{PL} was highest at 5 wt% emitter doping in mCBP (70%, a value comparable to that obtained in degassed toluene); this decreased to 59% when the film was exposed to air. In mCBP, ICzTRZ shows sky-blue emission at λ_{PL} of 479 nm, a maximum only slightly red-shifted compared to measurements in toluene and PMMA. Transient PL measurements in mCBP (Figure 5a) showed prompt fluorescence with a biexponential decay kinetics and an average τ_p of 8.7 ns [τ_1 = 4.5 ns (34%), τ_2 = 10.9 ns (66%)], and a delayed fluorescence with biexponential decay kinetics and an average τ_d of

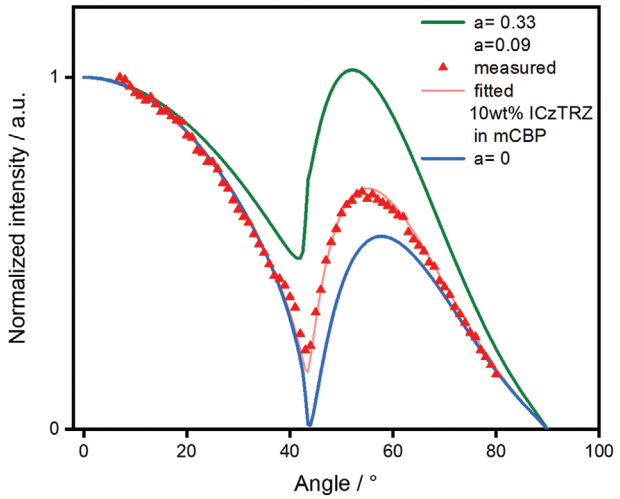

Figure 6. Angle-resolved photoluminescence measurement of an evaporated film of 10 wt% ICzTRZ in mCBP (red) and simulated graphs of isotropic (green) and horizontal (blue) orientation. The light red line shows a fit using the dipole emission model as described in detail in the Supporting Information, yielding an orientation parameter of 0.09.

Table 2. Orientation data obtained from angle-resolved photoluminescence measurements in different host materials.

Host	Doping [wt%]	a[a]	θ_h[b]	S[c]
mCP	10	0.12 ± 0.01	0.88	–0.32
mCBP	10	0.09 ± 0.02	0.91	–0.365
DPEPO	10	0.06 ± 0.02	0.94	–0.41

[a]Anisotropy factor; [b]Fraction of horizontal dipole ($\theta_h = 1 - a$); [c]Orientation order parameter, $S = (3a - 1)/2$.

121.09 µs [τ_1 = 19.1 µs (26%), τ_2 = 157.0 µs (74%)]. The multiexponential decay kinetics in both PMMA and mCBP reflect a heterogeneity of environments experienced by the ICzTRZ emitter. The TADF nature of the material was corroborated by measuring the temperature dependence of the delayed emission, which shows the characteristic increased contribution with increasing temperature (Figure 5b). The ΔE_{ST} was obtained from the onset of the prompt emission and phosphorescence spectra, measured at 77 K, with a value of 0.23 eV (Figure 5c). This value is in excellent agreement with the TDA-DFT calculations of 0.22 eV.

2.4. Orientation Measurements

The anisotropy factor (a) for ICzTRZ was measured in several OLED-relevant host materials (**Table 2**).[33] The doped films (10 wt% ICzTRZ in the host) were obtained via vacuum-deposition and the orientation of the emitter molecule was then measured using polarization- and angle-dependent luminescence spectroscopy, after which the data were analyzed by optical simulation (see Supporting Information for details). ICzTRZ presents a nearly completely horizontal orientation in all the host materials tested (see Figure S14, Supporting Information) with the best results obtained from the DPEPO doped film, with an anisotropy factor of 0.06. In the host mCBP (**Figure 6**), used for OLEDs, the orientation is a little less horizontal but the anisotropy value of 0.09—that is, 91% horizontal dipole contribution—is still among the best values reported in literature. Comparing the anisotropy factor for ICzTRZ to those of other carbazole- and triazine-based materials such as TCzTRZ[9] (a = 0.05), CC2TA[34] (a = 0.08), and 4CzTPN-Ph[35] (a = 0) we can observe the positive trend that large and flat molecules have on the anisotropy factor. Also, the longer shape of ICzTRZ led to a significant improvement in anisotropy values over the previously reported indolocarbazole emitters, IndCzpTr-1, and IndCzpTr-2 (a = 0.27 and 0.16, respectively).[11]

2.5. OLED Devices

We next fabricated OLEDs using the following optimized device structure: ITO/TAPC (40 nm)/TCTA (10 nm)/5 wt% ICzTRZ:mCBP (20 nm)/bis[2-(diphenylphosphino)phenyl] ether oxide (DPEPO) (10 nm)/TmPyPb (50 nm)/LiF (0.6 nm)/Al (100 nm). Indium tin oxide (ITO) is the semitransparent anode, 4,4′-cyclohexylidenebis[*N*,*N*-bis(4-methylphenyl)benzenamine] (TAPC) and tris(4-carbazoyl-9-ylphenyl)amine (TCTA) act as hole transport layers, 3,3′-di(9H-carbazol-9-yl)-1,1′-biphenyl (mCBP)

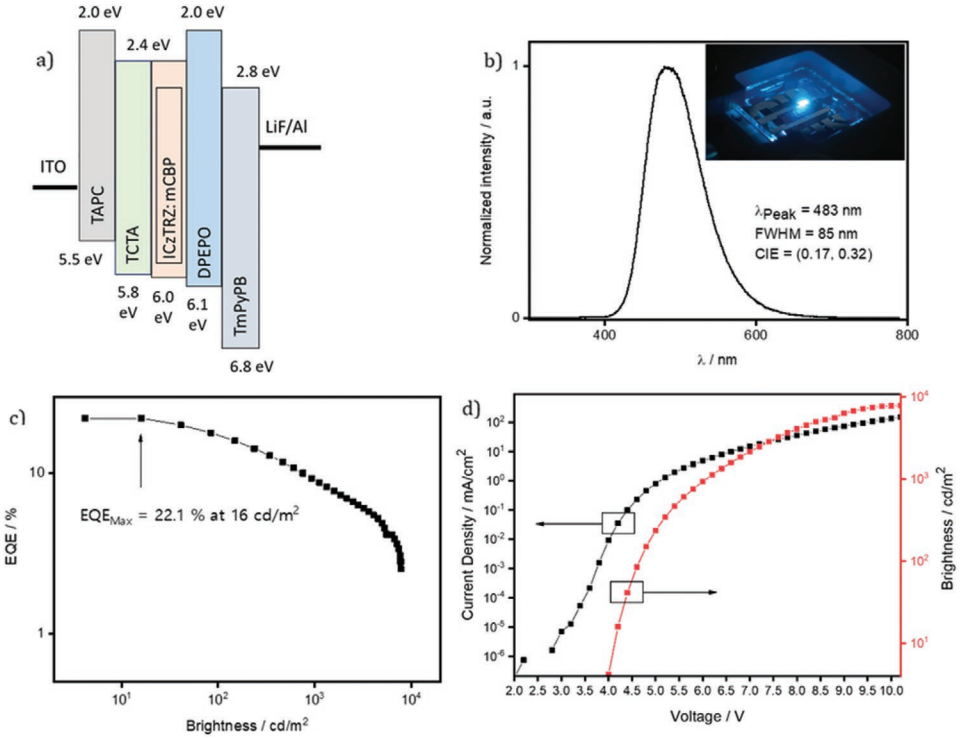

Figure 7. OLED data for ICzTRZ. a) Device structure; b) Electroluminescent spectra; c) External quantum efficiencies (EQE) versus brightness; d) Current density versus voltage versus brightness curves.

is the host, bis[2-(diphenylphosphino)phenyl] ether oxide (DPEPO) is the hole blocking layer, bis[2-(diphenyl)benzene (TmPyPB) acts as the electron transport material and LiF modifies the work function of the aluminum cathode (**Figure 7**a and Figure S15, Supporting information).

The electroluminescence (EL) spectrum shows sky-blue emission with a λ_{EL} at 483 nm and associated CIE chromaticity coordinates of (0.17, 0.32) (Figure 7b). Figure 7c shows the EQE versus luminance curve. The OLED shows an EQE_{max} of 22.1% at 16 cd m^{-2}. At 100 cd m^{-2}, the EQE_{100} value is 17.3%, a decrease of 22% from its maximum value. At 1000 cd m^{-2}, the EQE_{1000} values decrease to 9.1%. The device shows a low turn-on voltage (≈3.5 eV) and brightness level reaching 7805 cd m^{-2} (EQE = 2.5%) (**Table 3**). The out-coupling efficiency was inferred to be 31% based on the EQE_{max} value, the high Φ_{PL} of 70%, and considering the charge balance and exciton utilization efficiency are each 100% (see Device and Device Simulation in Supporting Information).

This is confirmed by optical simulations of the device EQE as discussed in detail in the Supporting Information (Figure S16, Supporting Information). As shown in **Figure 8**, using the above measured input parameters (PLQY and *a*) together with the optical constants of the given OLED layer stack, we predict an EQE of 21% in excellent agreement with the experimental result. Moreover, the simulation clearly demonstrates that at the given PLQY of 70%, a device EQE in excess of 20% is only possible due to the strong horizontal orientation of the emitter TDMs. If they were randomly oriented in the film, the device EQE would just be around 15%. Thus, we can infer that the molecules are strongly horizontally oriented in the device, in line with our thin-film orientation measurements.

Table 3. OLED performance metrics.

Device	V_{on} [a] [V]	EQE_{max} [b] [%]	EQE_{100} [b,c] [%]	EQE_{1000} [b,c] [%]	L_{max} [d] [cd m^{-2}]	CIE [e] (*x*, *y*)	λ_{EL} [f] [nm]
ICzTRZ	3.5	22.1	17.3	9.1	7805	0.17, 0.32	483

[a] V_{on}, turn on voltage; [b] EQE, external quantum efficiency; [c] Subscript 100 and 1000 refer to values taken at 100 and 1000 cd m^{-2}; [d] L, luminance; [e] CIE, in Commission Internationale de L'Éclairage coordinates; [f] EL, electroluminescence.

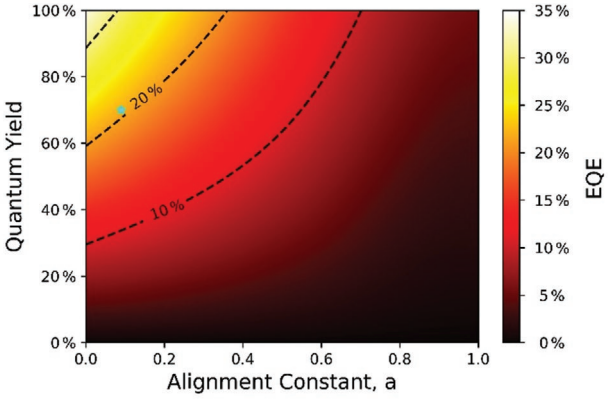

Figure 8. Simulated device efficiency of the given OLED layer stack, where the PL quantum yield (vertical axis) and the anisotropy factor (horizontal axis) are varied to visualize the influence of both parameters. The blue star marks the predicted EQE for the measured PLQY and the *a* parameter, which is in excellent agreement with the experimental result.

3. Conclusions

We have presented the first example of a di-functionalized indolocarbazole-based emitter in ICzTRZ. A particularly desirable feature of this material is that it displays almost complete horizontal orientation in three different host matrices, thereby enhancing light out-coupling in OLEDs made from it. This is likely due in part to the long stick-like shape of the emitter and the very small permanent dipole moment. The emitter also has high photoluminescence quantum yield. These properties led to a high-performance blue-emitting OLED (CIE coordinates of 0.17, 0.32), an EQE_{max} of 22.1%, and a luminance level reaching 7800 cd m^{-2}.

Supporting Information

Supporting Information is available from the Wiley Online Library or from the author. The research data supporting this publication can be accessed at https://doi.org/10.17630/fcb16565-94ec-449a-8749-94e70290d090.

Acknowledgements

Z.Z. and E.C. contributed equally to this work. This project was supported by the Helmholtz Association Program at the Karlsruhe Institute of Technology (KIT). The German Research Foundation (formally Deutsche Forschungsgemeinschaft DFG) in the framework of SFB1176 Cooperative Research Centre "Molecular Structuring of Soft Matter" (CRC1176, A4, B3, C2, C6) and the cluster 3D Matter Made to Order all funded under Germany's Excellence Strategy 2082/1-390761711 are greatly acknowledged for financial contributions. We acknowledge support from the Engineering and Physical Sciences Research Council of the United Kingdom (grant EP/P010482/1). Z.Z. acknowledges the financial support from China Scholarship Council (CSC, 201606890009) for his Ph.D. studies. Furthermore, E.C., B.A.N., P.S., W.B., and E.Z.-C. thank EU Horizon 2020 Grant Agreement No. 812872 (TADFlife) for funding.

Open access funding enabled and organized by Projekt DEAL.

Conflict of Interest

The authors declare no conflict of interest.

Keywords

acceptor–donor–acceptor emitters, blue emitters, horizontal orientation, indolocarbazole, organic light-emitting diodes, out-coupling effect, thermally activated delayed fluorescence emitters, triazine

Received: August 10, 2020
Revised: October 2, 2020
Published online: October 23, 2020

[1] Y. Liu, C. Li, Z. Ren, S. Yan, M. R. Bryce, *Nat. Rev. Mater.* **2018**, *3*, 18020.
[2] M. Y. Wong, E. Zysman-Colman, *Adv. Mater.* **2017**, *29*, 1605444.
[3] H. Uoyama, K. Goushi, K. Shizu, H. Nomura, C. Adachi, *Nature* **2012**, *492*, 234.
[4] F. B. Dias, T. J. Penfold, A. P. Monkman, *Methods Appl. Fluoresc.* **2017**, *5*, 012001.
[5] B. Milián-Medina, J. Gierschner, *Org. Electron.* **2012**, *13*, 985.
[6] D. Yokoyama, A. Sakaguchi, M. Suzuki, C. Adachi, *Org. Electron.* **2009**, *10*, 127.
[7] T. A. Lin, T. Chatterjee, W. L. Tsai, W. K. Lee, M. J. Wu, M. Jiao, K. C. Pan, C. L. Yi, C. L. Chung, K. T. Wong, C. C. Wu, *Adv. Mater.* **2016**, *28*, 6976.
[8] T. D. Schmidt, T. Lampe, M. R. D. Sylvinson, P. I. Djurovich, M. E. Thompson, W. Brütting, *Phys. Rev. Appl.* **2017**, *8*, 37001.
[9] S. Y. Byeon, J. Kim, D. R. Lee, S. H. Han, S. R. Forrest, J. Y. Lee, *Adv. Opt. Mater.* **2018**, *6*, 1701340.
[10] H. Kaji, H. Suzuki, T. Fukushima, K. Shizu, K. Suzuki, S. Kubo, T. Komino, H. Oiwa, F. Suzuki, A. Wakamiya, Y. Murata, C. Adachi, *Nat. Commun.* **2015**, *6*, 8476.
[11] S. Xiang, X. Lv, S. Sun, Q. Zhang, Z. Huang, R. Guo, H. Gu, S. Liu, L. Wang, *J. Mater. Chem. C* **2018**, *6*, 5812.
[12] J. H. Maeng, D. H. Ahn, H. Lee, Y. H. Jung, D. Karthik, *Dyes Pigm.* **2020**, *180*, 108485.
[13] D. Zhang, X. Song, M. Cai, H. Kaji, L. Duan, *Adv. Mater.* **2018**, *30*, 1705406.
[14] A. Endo, K. Sato, K. Yoshimura, T. Kai, A. Kawada, H. Miyazaki, C. Adachi, *Appl. Phys. Lett.* **2011**, *98*, 083302.
[15] K. Sato, K. Shizu, K. Yoshimura, A. Kawada, H. Miyazaki, C. Adachi, *Phys. Rev. Lett.* **2013**, *110*, 247401.
[16] D. Zhang, L. Duan, C. Li, Y. Li, H. Li, D. Zhang, Y. Qiu, *Adv. Mater.* **2014**, *26*, 5050.
[17] M. Liu, R. Komatsu, X. Cai, K. Hotta, S. Sato, K. Liu, D. Chen, Y. Kato, H. Sasabe, S. Ohisa, Y. Suzuri, D. Yokoyama, S. J. Su, J. Kido, *Chem. Mater.* **2017**, *29*, 8630.
[18] Q. Ai, J. Chai, W. Lou, T. Liu, D. Wang, C. Deng, C. Wang, G. Li, X. Liu, Z. Liu, Q. Zhang, *ACS Appl. Mater. Interfaces* **2020**, *12*, 6127.
[19] Y. J. Kang, J. Y. Lee, *Dyes Pigm.* **2017**, *138*, 176.
[20] G. Jiang, F. Li, X. Kong, J. Fan, Y. Song, C. K. Wang, L. Lin, *J. Lumin.* **2020**, *219*, 116899.
[21] N. Sharma, E. Spuling, C. M. Mattern, W. Li, O. Fuhr, Y. Tsuchiya, C. Adachi, S. Bräse, I. D. W. Samuel, E. Zysman-Colman, *Chem. Sci.* **2019**, *10*, 6689.
[22] S. Grimme, *Chem. Phys. Lett.* **1996**, *259*, 128.
[23] P. L. Santos, J. S. Ward, P. Data, A. S. Batsanov, M. R. Bryce, F. B. Dias, A. P. Monkman, *J. Mater. Chem. C* **2016**, *4*, 3815.
[24] T. Hosokai, H. Matsuzaki, H. Nakanotani, K. Tokumaru, T. Tsutsui, A. Furube, K. Nasu, H. Nomura, M. Yahiro, C. Adachi, *Sci. Adv.* **2017**, *3*, e1603282.
[25] H. Noda, H. Nakanotani, C. Adachi, *Sci. Adv.* **2018**, *4*, eaao6910.
[26] P. K. Samanta, D. Kim, V. Coropceanu, J. L. Brédas, *J. Am. Chem. Soc.* **2017**, *139*, 4042.
[27] Y. Wada, H. Nakagawa, S. Matsumoto, Y. Wakisaka, H. Kaji, *Nat. Photonics* **2020**, *14*, 643.
[28] M. A. El-Sayed, *Acc. Chem. Res.* **1968**, *1*, 8.
[29] D. Chen, P. Rajamalli, F. Tenopala-Carmona, C. L. Carpenter-Warren, D. B. Cordes, C. M. Keum, A. M. Z. Slawin, M. C. Gather, E. Zysman-Colman, *Adv. Opt. Mater.* **2020**, *8*, 1901283.
[30] P. L. Dos Santos, D. Chen, P. Rajamalli, T. Matulaitis, D. B. Cordes, A. M. Z. Slawin, D. Jacquemin, E. Zysman-Colman, I. D. W. Samuel, *ACS Appl. Mater. Interfaces* **2019**, *11*, 45171.
[31] Z. Li, W. Li, C. Keum, E. Archer, B. Zhao, A. M. Z. Slawin, W. Huang, M. C. Gather, I. D. W. Samuel, E. Zysman-Colman, *J. Phys. Chem. C* **2019**, *123*, 24772.
[32] M. Y. Wong, S. Krotkus, G. Copley, W. Li, C. Murawski, D. Hall, G. J. Hedley, M. Jaricot, D. B. Cordes, A. M. Z. Slawin, Y. Olivier, D. Beljonne, L. Muccioli, M. Moral, J. C. Sancho-Garcia, M. C. Gather, I. D. W. Samuel, E. Zysman-Colman, *ACS Appl. Mater. Interfaces* **2018**, *10*, 33360.
[33] B. A. Naqvi, M. Schmid, E. Crovini, P. Sahay, T. Naujoks, F. Rodella, Z. Zhang, P. Strohriegl, S. Bräse, E. Zysman-Colman, W. Brütting, *Front. Chem.* **2020**, *8*, 750.
[34] C. Mayr, S. Y. Lee, T. D. Schmidt, T. Yasuda, C. Adachi, W. Brütting, *Adv. Funct. Mater.* **2014**, *24*, 5232.
[35] M. Tanaka, H. Noda, H. Nakanotani, C. Adachi, *Appl. Phys. Lett.* **2020**, *116*, 023302.